# Atomic Force Microscopy (AFM) Studies of Liquid Crystalline Polymer (LCP) Surfaces

**S. A. C. GOULD,[1] J. B. SHULMAN,[1] D. A. SCHIRALDI,[2] M. L. OCCELLI[3]**

[1] W.M. Keck Science Center, The Claremont Colleges, Claremont, California 91711

[2] KoSa Corporation, Spartenburg, South Carolina 29304

[3] MLO Consultants, 6105 Blackwater Trail, Atlanta, Georgia 30328

*Received 18 November 1998; accepted 22 March 1999*

**ABSTRACT:** An atomic force microscope (AFM) operating in tapping or contact mode was used to study the surface topography and the molecular organization of Vectra-A and Vectra-B films. Large-scale ($15 \times 15$ $\mu$m) AFM images revealed that ribbonlike fibrils with a width/height $\gg 1.0$ are the dominant surface features of these liquid crystalline polymers (LCPs). The region of local disorder, surface debris, and interfibrillar debris as well as possible amorphous regions were observed in both LCP samples. Large fibrils, 5.0–10.0 $\mu$m in width, can be thought of as formed by smaller microfibrils capable of forming ordered structures. Microfibrils can bend upward, forming raised surface features; bend inward, originating cracks 1–2 $\mu$m wide on the film surface; or divide and subdivide into smaller units. Longitudinal and lateral stresses are believed responsible for the variation in fibril size, shape, and orientation. AFM images containing molecular-scale details showed that microfibrils consists of chains of molecules coiled around a central axis and that they can be only about 2.0 nm wide. These submicron surfaces consist of white spots (representing molecules) that can form ordered structures or that can cluster to form agglomerates distributed in a random manner. Submicron fibrils are believed to represent the LCP basic structural unit. AFM results indicate that the surface topography of Vecta-B is more ordered and uniform than is the one observed for Vectra-A. Seemingly, amorphous particles form debris on Vectra-A surfaces. Short rods oriented crosswise on the fibril surface are instead what increases the Vectra-B roughness. These LCPs can have a surface topography similar to the one observed in AFM images of a spiderweb. However, the spiderweb fibrils are formed by more uniform microfibrils that are oriented parallel to each other.  J Appl Polym Sci 74: 2243–2254, 1999

**Key words:** atomic force microscopy; liquid crystalline polymers; Vectra films

## INTRODUCTION

Atomic force microscopy (AFM) was first applied to polymer surfaces in 1988,[1] 2 years after Binnig and coworkers invented this type of scanning probe microscope.[2] AFM is frequently applied to polymer surfaces, principally to reveal the surface morphology, nanostructure, chain packing, and conformation while providing nanometer-scale features not accessible by other microscopic techniques. In a companion article,[3] AFM images were used to described poly(ethylene terephthalate) (PET) films with atomic-scale resolution and

*Correspondence to:* S. A. C. Gould (gould@physics.claremont.edu).

Journal of Applied Polymer Science, Vol. 74, 2243–2254 (1999)
 CCC 0021-8995/99/092243-12

it was shown that imaging forces can alter the PET film surface.[3] It was the purpose of this article to describe the surface topography of liquid crystal polymers, such as Vectra-A and Vectra-B, at the molecular-scale level using an AFM operating in contact or tapping mode.

Liquid crystalline polymers (LCPs) are highly oriented polymeric materials[4] used in a wide range of high strength-to-weight and elevated temperature applications and find special use in fine parts that can be precision-molded due to the unique rheology of such LCPs.[1] Vectra-A (commercialized by Hoechst-Celanese) is a thermotropic aromatic copolyester of approximately 27% 6-hydroxy-2-naphtholic acid (HNA) and 73% 4-hydroxybenzoic acid (HBA). Vectra-B is, instead, a 60% HNA, 20% terephthalic acid (TA), and 20% 4-aminophenol (AP) mixture.[5] The physicochemical properties of LCP are strongly dependent on the molecular orientation, order, and density. In addition to having different chemical compositions and physical properties, the two LCPs under study have different morphologies[6] and molecular orientation.[7] It has been shown that the molecular orientation distribution in LCPs is not constant. It reaches a maximum of 0.8–1.0 mm below the surface and a minimum near the center of the sample.[7–9]

In an effort to understand the effects of the various fabrication processes on the film structure, Vectra has been studied by a broad range of microscopic techniques that include transmission electron microscopy (TEM),[10] scanning electron microscopy (SEM),[11] field-emission SEM (FESEM),[12] and scanning tunneling microscopy (STM).[13] Images of the Vectra surface obtained by TEM and STM[10,11] revealed the presence of highly ordered structures consisting of microfibrils aligned with a preferred orientation. Information concerning the size, shape, and architecture of the microfibrillar structure requires imaging techniques with greater spatial resolution such as STM[13] or AFM.

Resolution is controlled by the size of the contact area between the tip and the polymer surface. Thus, the selection of a soft cantiliver is of paramount importance since the contact area can be minimized by reducing the tip radius or by reducing the applied force. It is for this reason that, in studies of polymer surfaces, low force and force-dependent imaging is performed.[6,14] In this study, images obtained in the contact-mode AFM were generated with a weak cantiliver having a force constant of 0.6 N/m.

## EXPERIMENTAL

Vectra-A and Vectra-B samples were obtained from the Ticona Corp. (Summit, NJ; Vectra is a registered trademark of the Ticona Corp.). These films were glued onto a steel disk with epoxy resin. After the glue dried, the AFM tip was carefully guided to the middle of the film, thus beginning the imaging session. The AFM used in this work was a Nanoscope III instrument (from Digital Instruments, Santa Barbara, CA) operating in contact or tapping mode. As always,[5] the AFM was calibrated using mica. The images presented in this article contain either 256 $\times$ 256 or 512 $\times$ 512 data points and were obtained within several seconds. The $Si_3N_4$ cantilivers (with an integral tip) had a length in the 60–120-$\mu$m range with a spring constant in the 0.1–0.6-N/m range. The typical force applied to obtain these images ranged from 1.0 to 100 nN. Several hundred images were examined using different cantilivers. The images in Figures 1–12 were Fourier transform-filtered. To avoid tip-related artifacts, imaging was performed with minimal (less than 10 nN) force and image features were reproduced in both the tapping and contact modes before being accepted as representative.

## RESULTS AND DISCUSSION

### Vectra-A

AFM images for the two Vectra samples are shown in Figures 1–10. Both surfaces are fairly flat, containing features irregular in size and shape. The large (15 $\times$ 15 $\mu$m) scale AFM image in Figure 1(A) for Vectra-A reveals a region of local disorder, characterized by irregular raised surface features about 200 nm in height. This image contrasts with the one in Figure 1(B), showing two large fibrils parallel to each other. Cross-sectional analysis of the image in Figure 1(B) reveals that the average fibril height ($h$) is the same (2.0 nm) and that the width ($w$) is 4.2 and 3.0 $\mu$m, respectively. The lateral (center-to-center) distance between the fibrils is 3.0–3.5 $\mu$m. The white arrow in Figure 1(B) points to microfibrils with widths in the 0.30–0.40-$\mu$m range, which are the main component of the large fibril shown in this image. Although fibrils have been observed to vary in size, their $w/h$ ratio is always much greater than 1.0. Patterns of this type could be attributed to artifacts resulting from interference between the incident and reflected light from

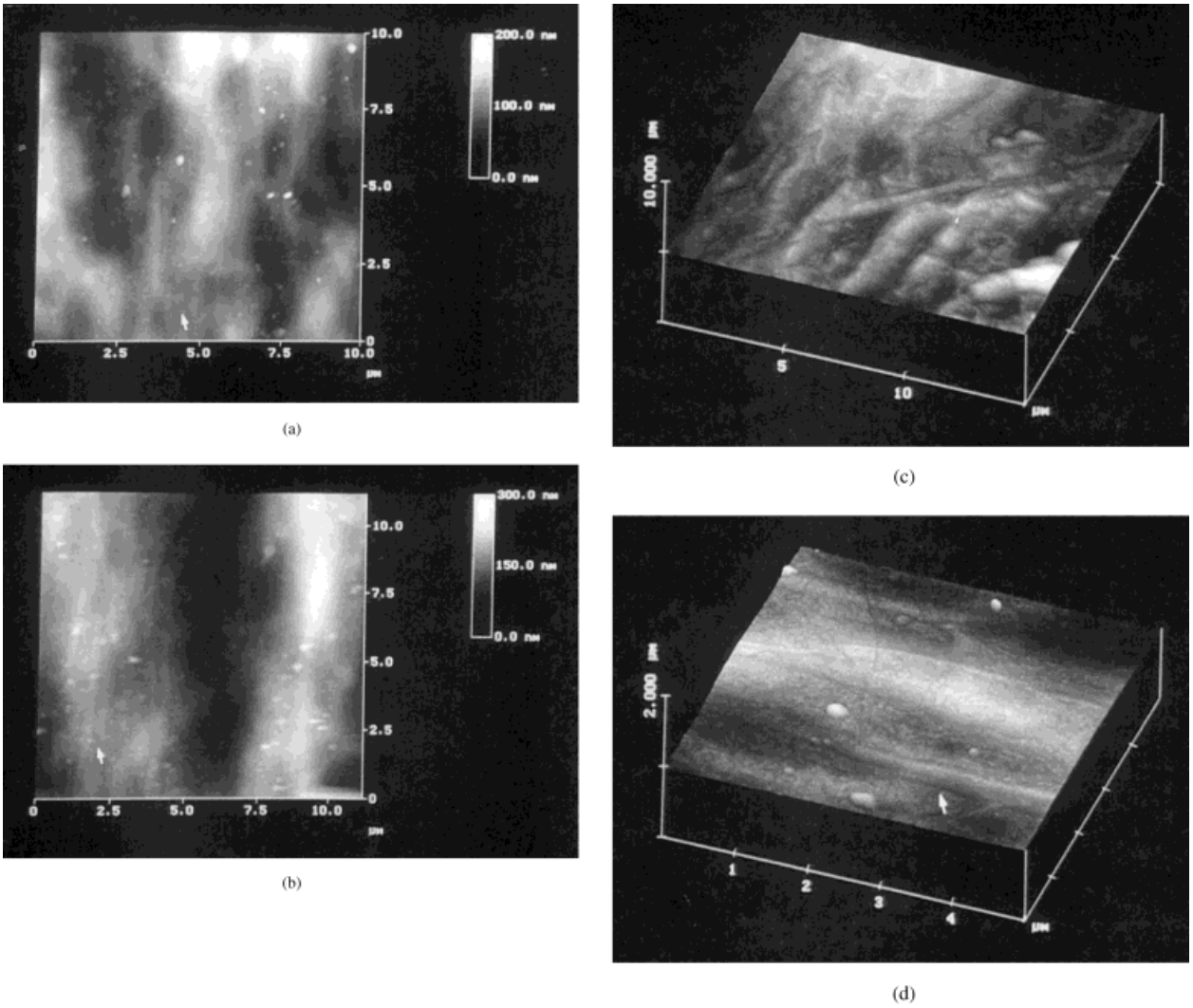


**Figure 1** Large-scale tapping mode AFM images in air of Vectra-A showing (a) top view of an amorphous domain of the surface and (b) fibril size and shape and (c) side-view image showing the boundary between fibrils and amorphous zones and (d) partial fibrils into microfibrils (white arrow). The white spots on these images represent surface debris.

the sample surface.[15] However, the pattern in Figure 1(B) was obtained with the AFM operating in the contact or tapping mode and it was observed also in TEM and SEM studies.

Microfibrils are not always are seen as components of larger units. In fact, fibrils can meet and fuse into what appears to be amorphous regions that are flat and featureless [Fig. 1(C)]. Figure 1(D) shows another example of a fibril 2.2 $\mu$m in diameter, resulting from the agglomeration of much smaller microfibrils 0.45 $\mu$m wide [see white arrow in Fig. 1(D)]. In Figure 1(A–D), the debris appear to contaminate the Vectra-A surface. The appearance of debris is a fairly common occurrence in this sample. Oftentimes, the debris appears as large granules (0.35 $\mu$m in width and 0.06 $\mu$m in height) on the film surface, as in Figure 2(A), or as smaller granules (0.030 $\mu$m in size) between fibrils, as shown in Figure 2(B). The nature of the debris is unknown at the present time. Possibly, the debris could be composed of highly crosslinked materials produced during the high-temperature synthesis of the polymer. In Vectra-A, surface impurities can also assume the form of irregular ribbons that meander on and off the fibril surface (see Fig. 3).

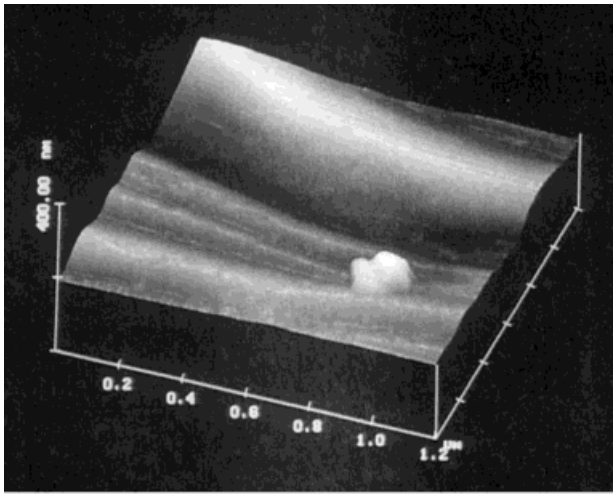


(a)

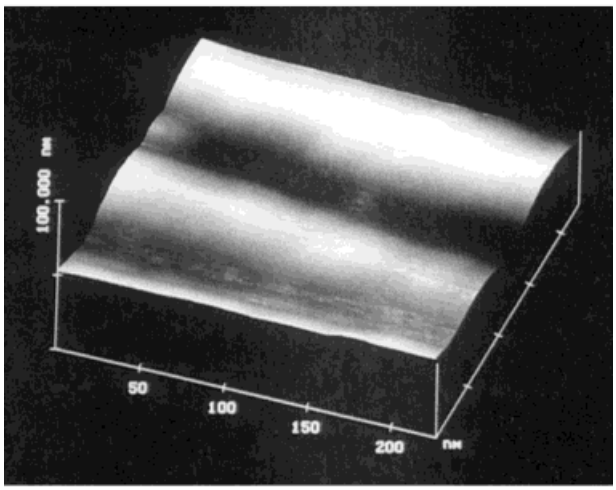


(b)

**Figure 2** Tapping-mode AFM images in air of Vectra-A showing (a) amorphous debris on the fibril surface and (b) between the fibrils.

Structural details of a fibril can be observed in Figure 4(A). In fact, this fibril, about 2.5 $\mu$m wide, appears to consist of a bundle of microfibrils with variable diameters in the 0.16 to 0.40 nm range; their heights are in the 0.01–0.04-$\mu$m range. Microfibrils can twist, remain of uniform thickness, or split into smaller components [Fig. 4(A)]. In addition, microfibrils can bend upward and agglomerate or twist and intertwine to form a surface feature 0.15 $\mu$m raised above the film surface or can form larger fibrils on the film surface [see white arrow in Fig. 4(B)]. Furthermore, fibrils have been observed to bend into the film surface, producing cracks 1.5 $\mu$m wide and 0.8 $\mu$m deep [Fig. 4(C)]. These features (microfibril splitting, twisting, bending) were also observed while operating the AFM in the contact mode.

In Figure 5(A), fibrils with an average size of 0.070 $\mu$m spaced 0.13 $\mu$m apart can be easily observed. Some of the fibrils bend and disappear from the surface while others are separated by featureless domains. In contrast, the surface in Figure 5(B) appears composed by fibrils with an average width of 0.17 $\mu$m, which, in this case, bend, generating an indentation on the film surface. This image contains a good example of a fibril splitting into two and three smaller subunits. The details shown in Figure 6 were already observed by SEM. This 5 $\times$ 5-$\mu$m Vectra-A image represents fibrils (with an average width of 0.90 $\mu$m) as a collection of long-range staking of platelets 0.14 $\mu$m thick.

Nanometer-scale details of a microfibril can be observed in Figure 7. In Figure 7(A), microfibrils 2.0 nm in width appear as raised surface features

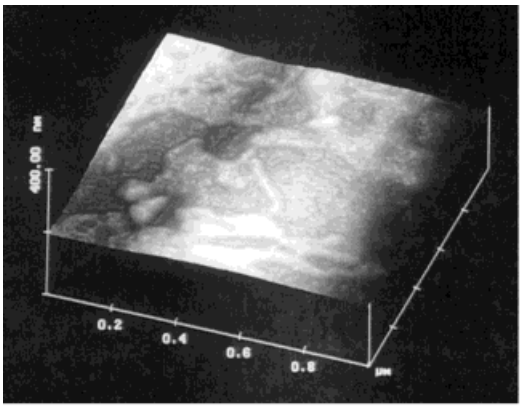


(a)

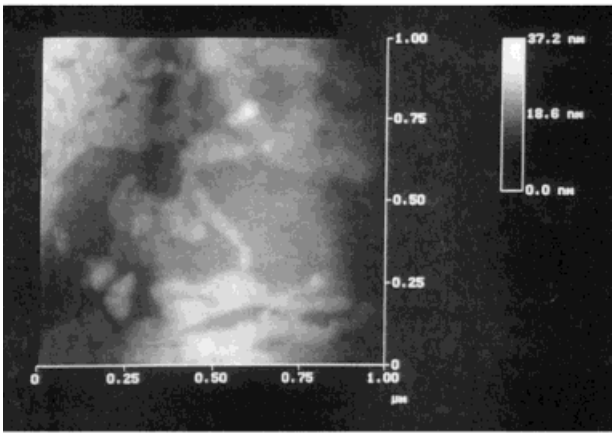


(b)

**Figure 3** Tapping-mode AFM images in air of Vectra-A showing ribbonlike surface debris meandering across the fibril surface: (a) side view; (b) top view.

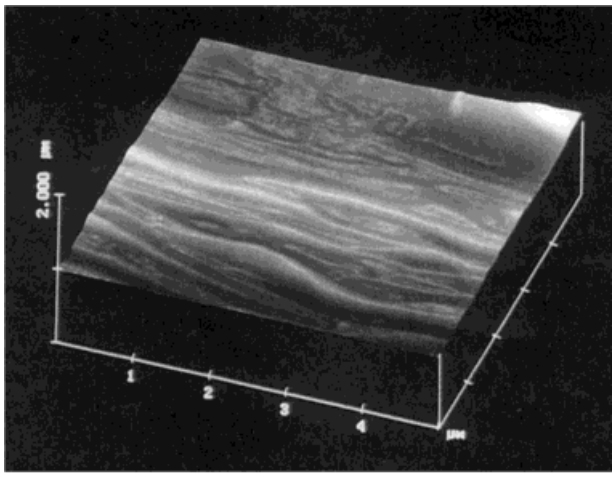


(a)

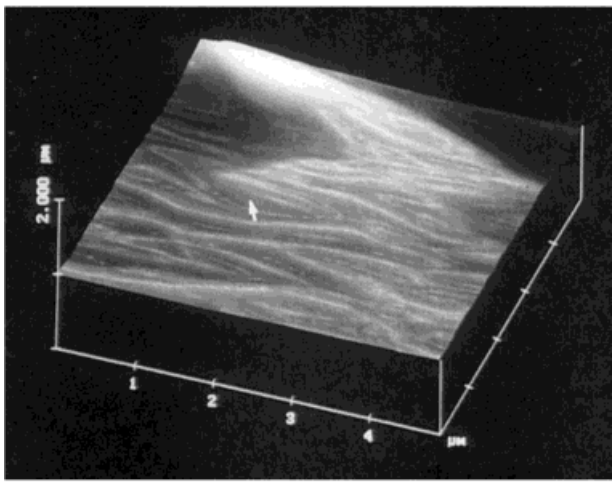


(b)

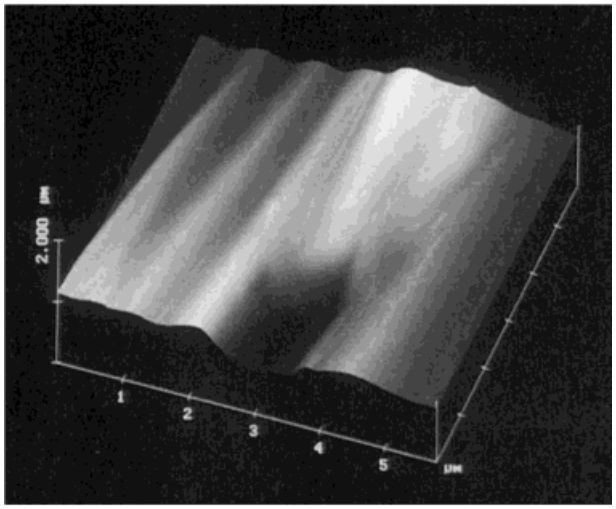


(c)

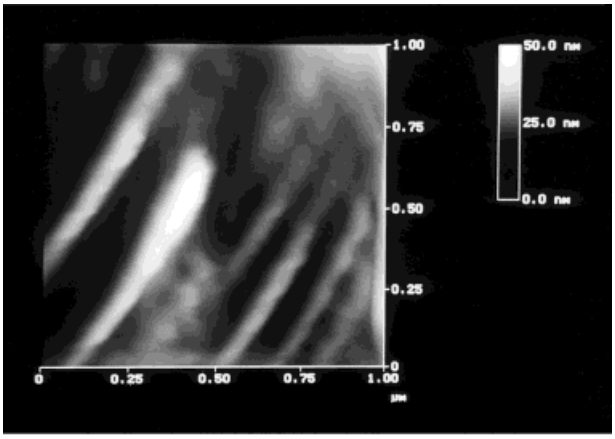


(a)

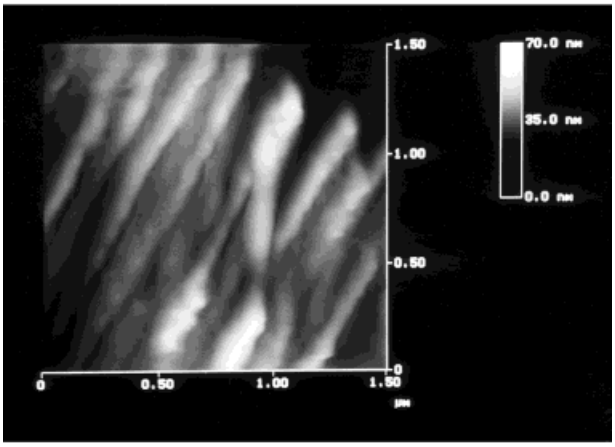


(b)

**Figure 5** Contact-mode AFM images in air of Vectra-A showing (a) variations in fibril size and fibrils leaving the film surface and (b) fibril decomposition into three or two components and bending of fibrils with the formation of kinks on the film surface.

0.5 nm in height consisting of chains (or agglomeration) of molecules. Similar details can also be seen in a larger microfibrils 5 nm wide [see Fig. 7(B)]. Atomic-scale details of these features are shown in the 6 × 6-nm images in Figure 7(C–D). White spots about 1 nm in size (and believed to

**Figure 4** Large-scale tapping-mode AFM images in air of Vectra-A showing (a) microfibril agglomeration into larger fibrils, (b) surface discontinuities (white arrow) in fibrillar domains, and (c) fibrils leaving the film surface and formation of surface openings.

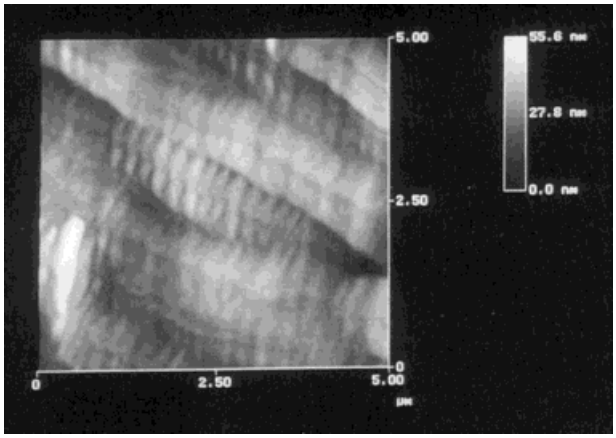


**Figure 6** Contact-mode AFM images in air of Vectra-A showing the long-range staking of platelike components and the forming of different-size fibrils.

represent molecules or molecular clusters) form chains of variable length that can orient parallel to each other to form regions characterized by a well-defined pattern [see Fig. 7(C)]. Alternatively, these white spots can cluster together to originate zones void of repeat distances and order [Fig. 7(D)].

### Vectra-B

The surface of Vectra-B exhibits features similar to those seen in Vectra-A. However, its surface appears to be more ordered and less contaminated with debris. The large (15 $\times$ 15 $\mu$m) image in Figure 8(A) shows a fairly flat amorphous region with several surface indentations responsible for a surface roughness of 9.6 nm. Amorphous domains can contain crevices and valleys, probably the result of longitudinal and lateral forces generated during the materials' preparation.

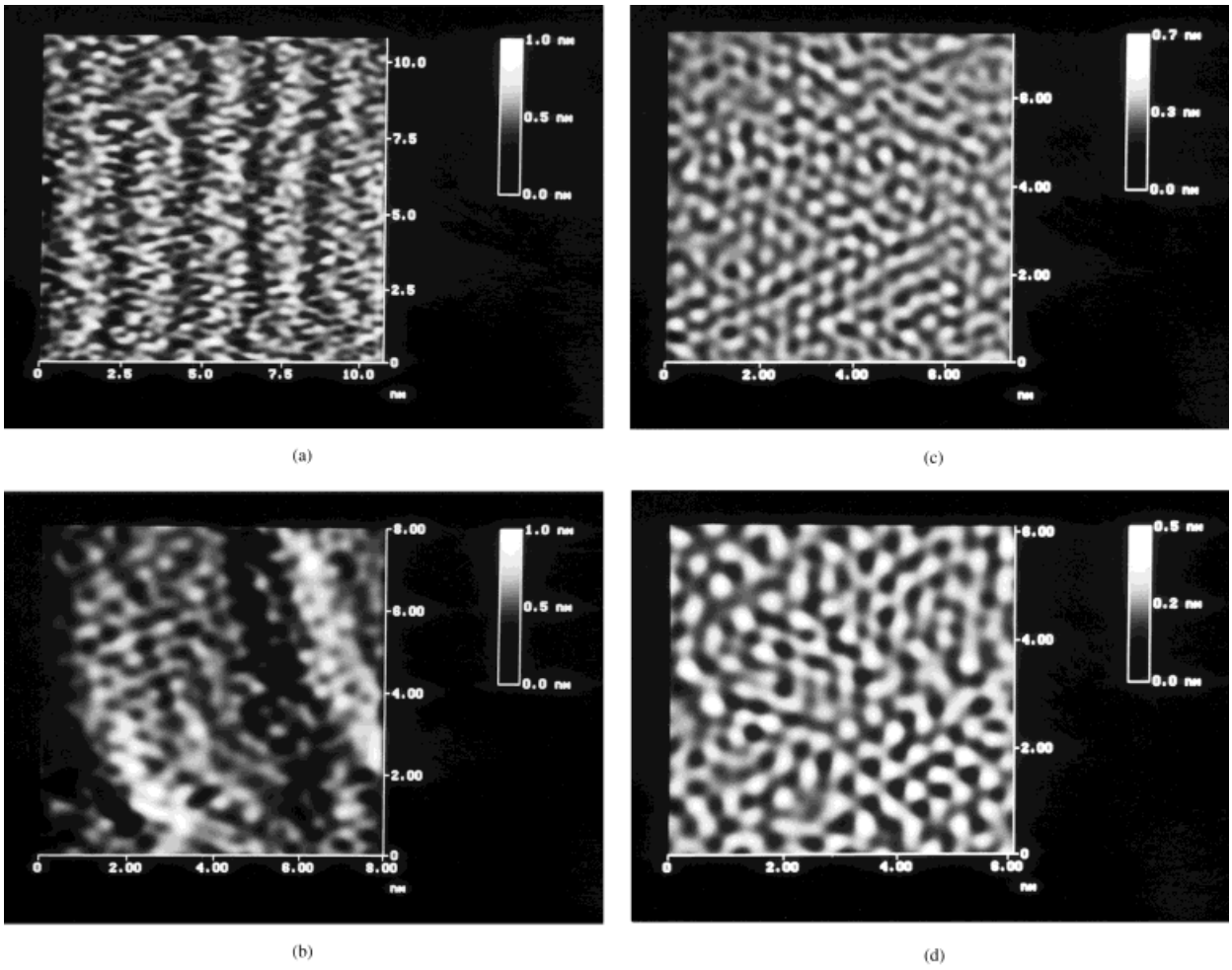


**Figure 7** Molecular-scale contact-mode AFM images in air of Vectra-A: (a) top view of several submicron fibrils; (b) variations in submicron fibril sizes; (c,d) atomic-scale details of a submicron fibril surface.

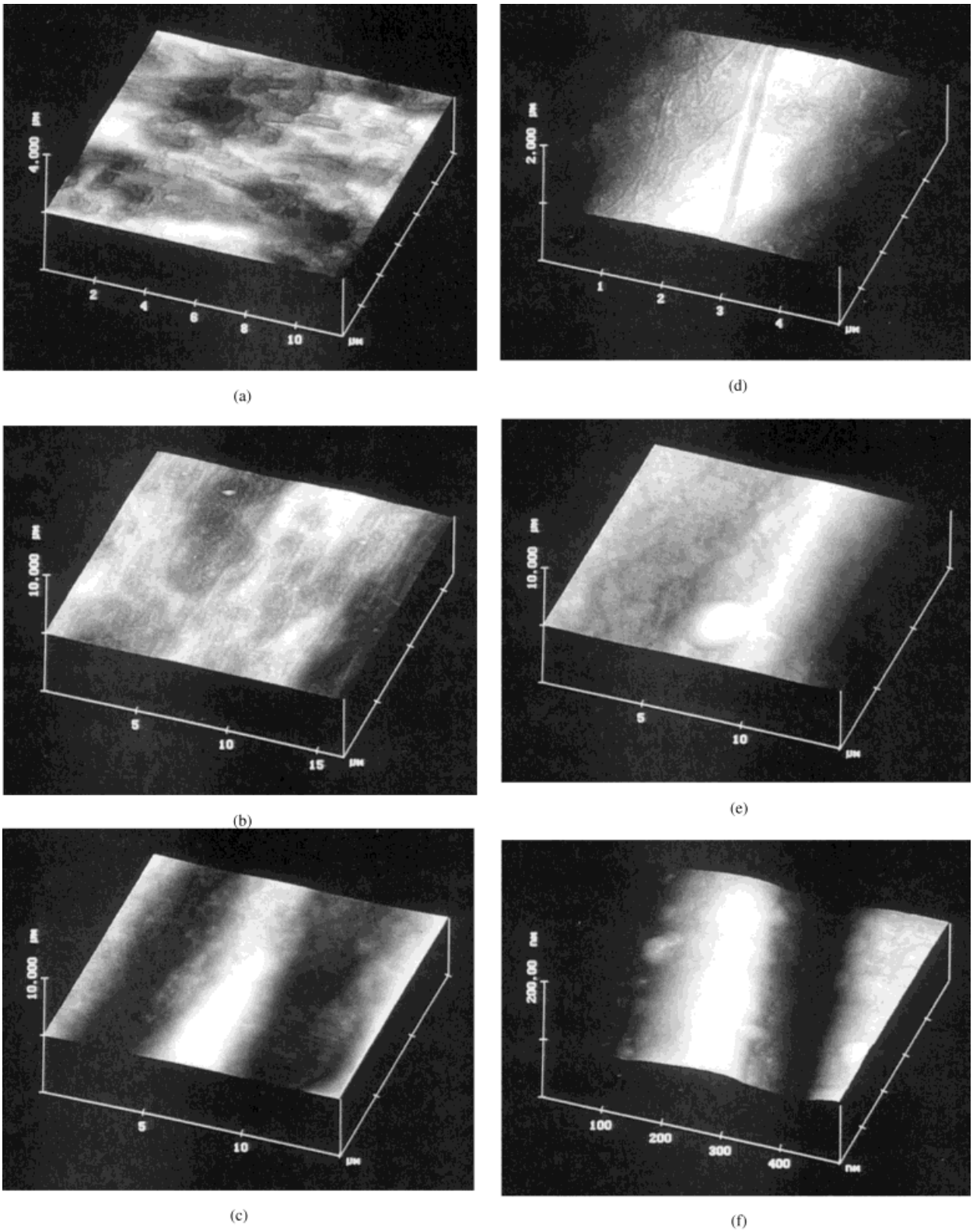


**Figure 8** Large-scale tapping-mode AFM images in air of Vectra-B showing (a) top view of an amorphous domain of the surface, (b) a ribbonlike fibril; (c) side-view image showing a different fibril, (d) raised surface feature on the fibril surface, (e) a large particle on the fibril surface, and (f) distribution of smaller debris on the fibril surface.

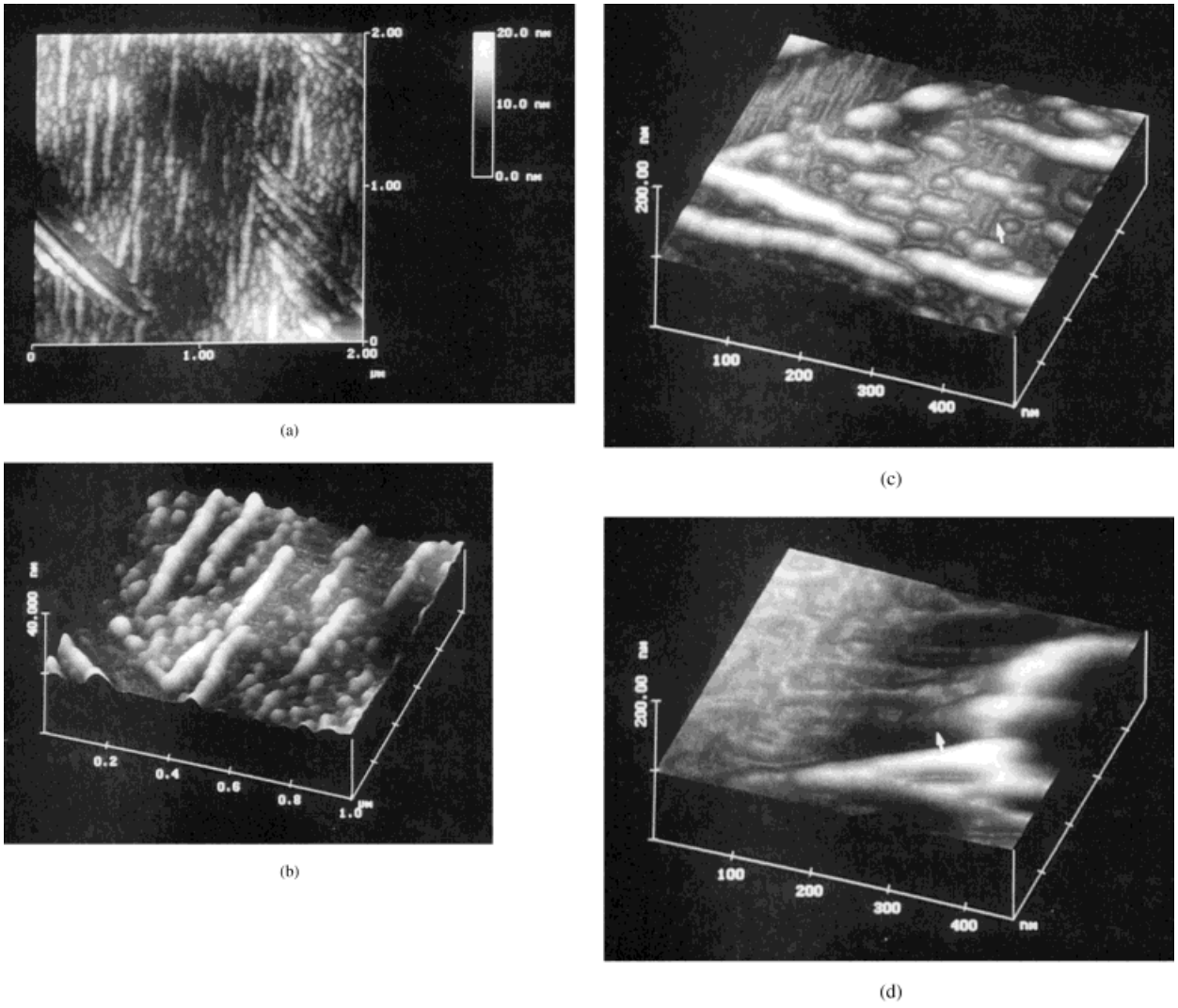


**Figure 9** Tapping-mode AFM images in air of Vectra-B rodlike debris on the surface: (a) top view, (b) side view, and (c) image showing the orientation of these rodlike materials with respect to the fibril direction. In (d), fibrils bend upward and cluster together to form surface irregularities.

More common are regions showing large fibrils having different widths and heights (with $w/h >> 1.0$). An example of a typical ribbonlike fibril 7.5 $\mu$m wide is shown in Figure 8(B), while differences in fibril height can be observed in Figure 8(B). In the Vectra-B samples, fibrils sometimes appear to contain, on their surface, microfibrils (0.18 $\mu$m wide) running lengthwise as in Figure 8(D) or large amorphous particles (3.2 $\mu$m in size and 0.16 $\mu$m thick) as in Figure 8(E). Fibrils decorated with debris, as shown in Figure 8(F), are not uncommon.

The surface details in Figure 9(A–B) were observed only with the Vectra-B sample. Figure 9(A) is a top-view image indicating the presence of relatively short rods (about 0.060 $\mu$m wide) irregular in size and shape covering the surface. The side-view image in Figure 9(B) highlights the height of these rods and shows that they may be the result of the condensation of amorphous particles on the LCP surface. Although these rods do not appear to have a preferred orientation, they tend to align themselves across the fibril direction [see white arrow in Fig. 9(C)]. The $0.5 \times 0.5$-$\mu$m image in Figure 9(D) shows the decomposition of raised surface fibrils into microfibrils on the Vectra-B surface.

Nanometer-scale details of four microfibrils are shown in the $40 \times 40$-nm image in Figure 10(A). As seen for Vectra-A, microfibrils appear to be

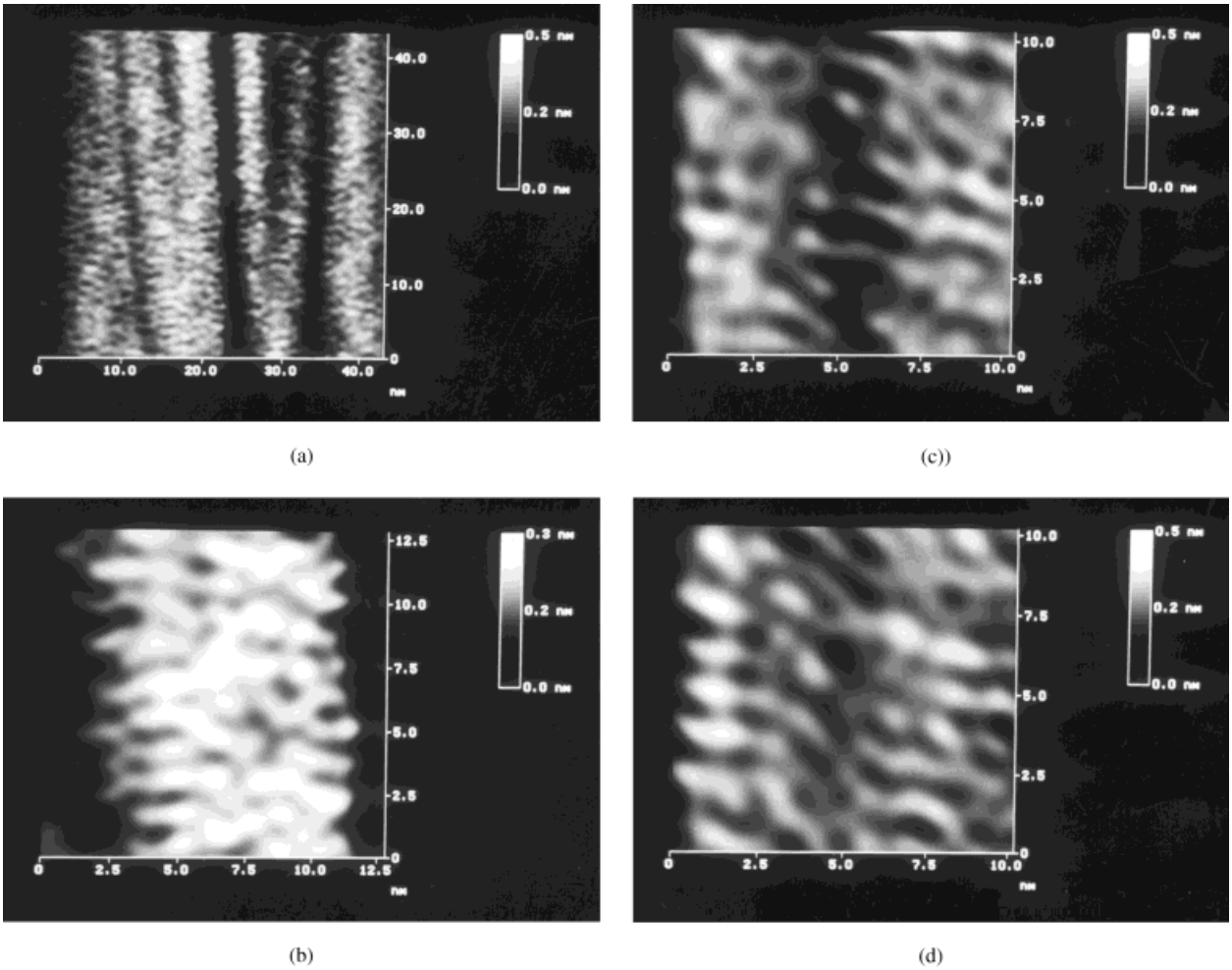


**Figure 10** Molecular-scale contact-mode AFM images in air of Vectra-B: (a) fibrils with nanometer dimensions; (b) molecular details of the microfibril indicated by the white arrow in (a) before splitting, (c) during splitting, (d) after splitting.

formed by chains of molecules that, surprisingly, align themselves normal to the microfibril direction. The white arrow in Figure 10(A) points to the decomposition of a microfibril about 8 nm wide into two smaller components. Before splitting, the microfibril surface appears to be formed by chains of molecules coiled around a central axis [Fig. 10(B)]. As the separation begins, these chains tend to stretch along the separation direction. Then, bond breaking causes the chains to separate and to form two new fibrils [Fig. 10(C)].

In Figure 11, AFM images of a spiderweb surface[16,17] show a good similarity with the fibrils observed in Figure 4(A,B). However, in contrast to LCP, fibrils in a spiderweb filament appear to be formed by a well-ordered agglomeration of smaller microfibrils fairly regular in size and shape. This structural order and homogeneity could play an important role in defining the strength of these materials.

## Image Artifacts

With hard surfaces such as clays,[18,19] image generation is dominated by the surface topology, by the tip geometry, and, when working in air, by the meniscus force of a water film on the surface.[20] This force and the large contact area between the tip and the surface are the main source of image artifacts while studying hard surfaces. Nonetheless, today, these types of surfaces are routinely imaged with molecular resolution.

On the other hand, with soft surfaces such as PET films,[3] the probing tip can generate irreversible indentation of the surface, thus modifying the sample surface topography.[3,21] Furthermore, as a sample softness increases, resolution decreases, indicating that the elasticity of the surface affects image formation in soft samples.[22,23] Thus, the viscoelastic properties of the samples provides an additional parame-

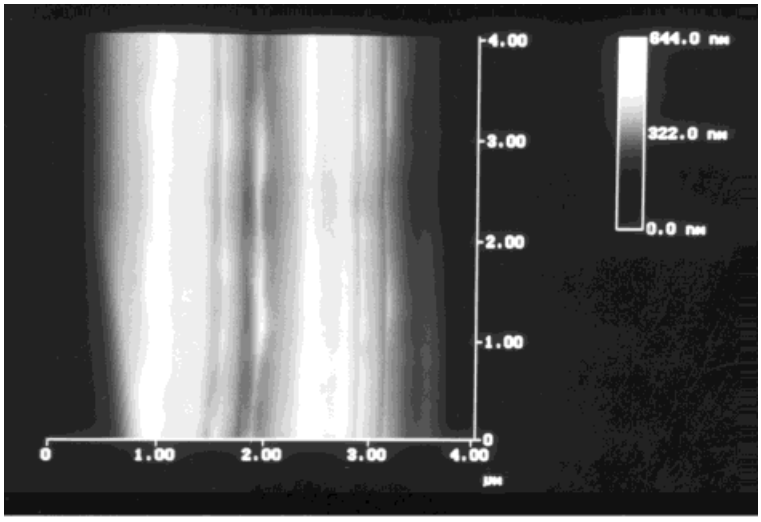


(a)

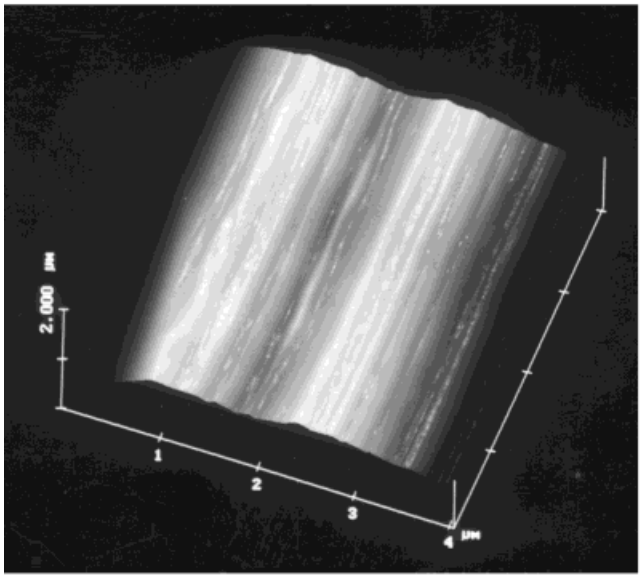


(b)

**Figure 11** Large-scale tapping-mode AFM images in air of a spiderweb filament: (a) top view; (b) side view.

ter that may influence image formation and the generation of image artifacts.

For highly reflective and soft surfaces such as those of Vectra films, interference between the incident and reflected light from the surface can produce a sinusoidal pattern on the image (with a period in the 1.0–2.5-$\mu$m range) totally unrelated to the sample surface topography.[15] The large-scale image in Figure 12(A) was obtained with the AFM operating in the contact mode using $Si_3N_4$ cantilevers. The laser was aimed so that only a small fraction of its total light output (approximately 1/10th of the maximum amount) was reflected from the cantilever. As a consequence, a greater percentage of the signal being measured by the multisegment photodiode was a result of the interference from the light reflected by the sample and the light reflected off the cantilever. One unusual aspect of this artifact is that its size and shape remains constant even after changing the scan speed, the scan size (imaging at various resolutions), and the scan direction. The image in Figure 12(B) shows that the artifact can be eliminated simply by adjusting the aim of the laser

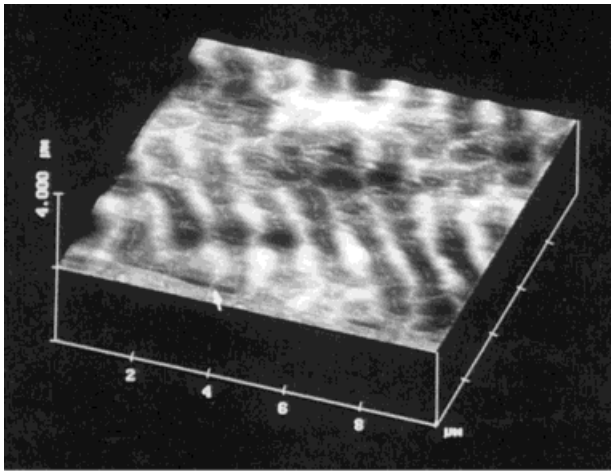


(a)

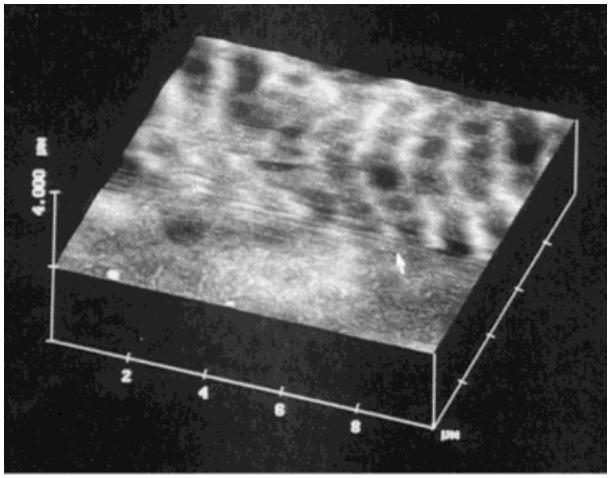


(b)

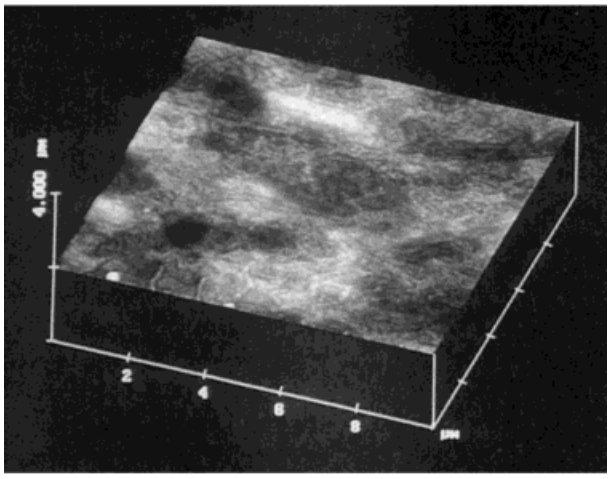


(c)

**Figure 12** Contact-mode AFM images in air of Vectra-A showing (a) image artifacts induced by optical interference, (b) the effects of eliminating optical interference during the imaging acquisition, and (c) an artifact-free image.

beam so that a greater percentage of the light reflects off the cantilever and not from the surface. The real image can then be seen in Figure 12(C). Optical interference artifacts are less common when operating the AFM in the tapping mode.

## SUMMARY AND CONCLUSIONS

An AFM operating in a contact mode can generate images containing structural details of Vectra film surfaces that are beyond the resolution capability of conventional electron microscopes such as TEM and SEM. In fact, although evidence of the existence of an atomic-scale fibril consisting of two molecular chains[2] could not be obtained, molecular-scale AFM images have shown that microfibrils 2 nm in size are formed by a chain of atoms or molecules coiled around a central axis . White spots about 1.0 nm wide (and believed to represent molecules or molecular clusters) form chains with variable lengths and with well-defined repeat distances. These regions of local order are separated by regions in which these white spots form clusters that are distributed in a nearly random manner. Microfibrils 2 nm wide are believed to represent the film's basic structural unit.

Large-scale AFM images have revealed that these LCP surfaces consist of amorphouslike regions and ordered domains in which fibrils having width ($w$) and height ($h$) such that $w/h \gg 1$ are the dominant feature of the surface. Thus, these fibrils posses a ribbonlike instead of a tubular geometry. Fibrils 5–10 $\mu$m wide have been observed to consist of bundles of microfibrils and those microfibrils can subdivide into smaller units; the aspect ratio of width to height always remains $>> 1$. These observations lend support to the belief that submicron fibrils are probably the building blocks responsible for the LCP mechanical properties.[24,25]

Local order is, in general, not uniform and microfibrils can vary in size, appearance (possibly due to stretching), and direction. Whether fibrils result from the self-assembly of the polymer components (chains of molecules) or from deformation during film preparation remains a subject of debate.

AFM images indicate that, on the local scale, the surface of Vectra-B is somewhat more ordered than is the surface of Vectra-A. It is possible that this additional order is the result of some degree of self-assembly, via hydrogen bonding, of the

aminophenol repeat units. In the Vectra-A film, small amorphous particles in the form of granules or in the form of thin ribbons decorate the fibril surface. In contrast, on the Vectra-B surface, short rods of variable length appear crosswise on the fibril surface, increasing its roughness. Optical interference artifacts can be avoided by operating the AFM in a tapping mode (at the expense of resolution) or by operating in a contact mode by maintaining the laser beam on the AFM cantiliver.

## REFERENCES


1. Binnig, J.; Rohrer, H.; Gerber, C.; Weibel, E. Phys Rev Lett 1983, 50, 120.
2. Albrecht, T. R.; Dovek, M. M.; Lang, C. A.; Grutter, P.; Quate, C. F.; Kuan, S. N. J.; Frank, C. W.; Pease, R. F. W. J Appl Phys 1988, 64, 1178.
3. Gould, S. A. C.; Schiraldi, D. A.; Occelli, M. L. J Appl Polym Sci 1997, 4, 1237.
4. Kirk-Othmer Encyclopedia of Chemical Technology; Wiley: New York, 1985; Vol. 15, p 372.
5. Sawyer, L. C.; Chen, R. T.; Jamieson, M. G.; Musselman, I. H.; Russel, P. E. J Mater Sci 1993, 28, 225.
6. De Neve, T.; Navard, P.; Kleman, M. J Rheol 1993, 37, 515.
7. Dreher, S.; Zachmann, H. G. Macromolecules 1995, 28, 7071.
8. Pirnia, A.; Sung, C. S. P. Macromolecules 1988, 21, 2699.
9. Bengel, H.; Magonov, S. N.; Cantow, H.-J.; Hillebrecht, H.; Thiele, G.; Liang, W.; Whangbo, M.-H. Surf Sci Lett 1995, 84, 111.
10. Sawyer, L. C.; Jaffe, M. J Mater Sci 1986, 21,1897.
11. Viney, C.; Donald, A. M.; Windle, A. H. J Mater Sci 1983, 18, 1136.
12. Sawyer, L. C.; Grubb, D. T. In Polymer Microscopy; Chapman and Hall, London, 1987.
13. Musselman, I. H.; Russel, P. E.; Chang, R. T.; Jamieson, M. G.; Sawyer, L. C. In Proceedings of the 12th International Congress on Electron Microscopy, Seattle, August 1990; Bailey, W., Ed.; San Francisco Press: San Francisco, 1990; p 866.
14. Bengel, H.; Cantow, H.-J.; Magonov, S. N.; Monconduit, L.; Evain, M.; Whangbo, M.-H. Surf Sci Lett 1994, 321, L170.
15. Digital Instrument SPM Training Notebook, 1996; p 47.
16. Nguyen, A. N.; Moore, A. M. F.; Gould, S. A. C. In Proceedings of the 52nd Annual Meeting of the Microscopy Society of America; Bailey, G. W.; Garratt-Reed, A. J., Eds.; San Francisco Press, San Francisco, 1994; p 1056.
17. Tran, K.; Spagna, J.; Shulman, J.; Moore, A. M. F.; Gould, S. A. C. Paper presented at the Silk Symposium, UV Charlottesville, VA, June 14–17, 1998.
18. Hartman, H.; Sposito, G.; Yang, A.; Manne, S.; Gould, S. A. C.; Hartman, P. K. Clay Clay Miner 1990, 38, 337.
19. Occelli, M. L.; Drake, B.; Gould, S. A. C. J Catal 1993, 142, 337.
20. Israelachvili, J. N.; Pashley, R. M. Nature 1983, 306, 249.
21. Radmacher, M.; Tillman, R. W.; Fritz, M.; Gaub, H. E. Science 1992, 257, 1900.
22. Wawkuschewski, A.; Cantow, H.-J.; Magonov, S. N. Adv Mater 1994, 6, 476.
23. Dreher, S.; Seifert, S.; Zachmann, H. G.; Moszner, N.; Mercoli, P.; Zanghellini, G. J Appl Polym Sci 1996, 67, 531.
24. High Performance Polymers; Baer, E.; Moet, A., Eds.; Hanser: New York, 1991.
25. Frey-Wyssling, A. Science 1954, 119, 80.